POLITECNICO
MILANO 1863

Aircraft Landing Optimization

Bartesaghi Alessandro
D'Aleo Damiano
Rocca Luca
Vanacore Luigi

Contents

1 Introduction **1**

2 Modeling and Simulation **2**
2.1 System description and hypothesis 2
2.2 Flight Model 2
2.2.1 Aerodynamic Coefficients 4
2.3 Ground Model 5
2.4 Combined Switching Model 6
2.5 Simulation 7
2.5.1 Results 7

3 Finite Horizon Optimal Control **8**
3.1 Optimization Problem 8
3.2 Main issues of the optimization problem 9
3.3 Final Solution 10
3.3.1 Unconstrained Optimization 10
3.3.2 Line Search Parameters 11
3.3.3 Barrier Functions 11
3.3.4 Unconstrained Optimization Results 13
3.3.5 Constrained Optimization 14
3.3.6 Constrained Problem Refinements 14
3.3.7 Results and Observations 15

4 Conclusion **18**

5 Appendix **19**

1 Introduction

Air travel connects people across continents, facilitating business, tourism, and exploration. While renowned for its speed and safety, the most critical moment of any flight remains the landing. This transition from cruising altitude to touchdown demands immense precision and coordination, impacting both passenger comfort and aircraft lifespan.

This report delves into the intricacies of aircraft landing, focusing on a specific challenge: reducing accelerations and enhancing passenger comfort.

Through modeling and analysis, opportunities have been identified to optimize the landing process. The goal is to develop solutions that minimize vibrations and ultimately achieve smooth, comfortable touchdowns.

By addressing these challenges, the aim is to ensure a safer, more comfortable, and more efficient air travel experience for passengers and airlines alike.

2 Modeling and Simulation

2.1 System description and hypothesis

The landing procedure of an aircraft is mainly characterized by two phases:

- Descent Phase: The aircraft is aligned with the runway and has to gradually lower its altitude in order to land.
- Ground Phase: The aircraft has made contact with the landing strip and has to lower its speed to complete the landing procedure without overshooting and violating the constraint imposed by the runway length

Since the aircraft exhibits two completely different behaviors in these two phases, two dynamical models have been developed to fully capture the dynamics of the aircraft both during the descent phase and the deceleration phase after touchdown. In order to design both models, some assumptions have been made and are reported in the following:

1. *2D Planar Motion*: since the landing procedure is mainly concerned with a planar movement of the aircraft, only its longitudinal, vertical and pitching dynamics have been modeled.
2. *Directly Controlled Aerodynamic Coefficients*: to simplify the complex relation between the control surfaces of the airplane and the generated aerodynamic forces, the control inputs were assumed to modify the drag and lift coefficients directly as described in 2.2.1.
3. *Ideally Controlled Pitch Dynamics during Flight Mode*: since all aircraft are equipped with flight control systems, the presence of these has been exploited to model the pitching dynamics of the plane. The relation between cloche command and aircraft pitching has been modeled as a second-order asymptotically stable dynamical system with suitably chosen natural frequency and damping ratio.
4. *Neglected wind disturbance*: for simplification, the influence of wind on the aircraft's aerodynamics have been omitted, resulting in a scenario without external disturbances.

The two models have been then derived using Lagrange's equations and have been named "Flight Model" and "Ground Model" respectively. Their equations of motion are reported in Subsections 2.2 and 2.3.
Dynamic parameters for commercial aircraft are usually confidential. In order to derive the parameters for the two models, the ones in [1] and [2] referring to a fighter jet have been used. Notice that the whole treatise can also be extended to a commercial aircraft.

2.2 Flight Model

The in-flight model was conceived to be a rigid body moving in a plane on which aerodynamic, gravitational and propulsion forces act:

$$\begin{cases} M\ddot{X}(t) = T(t)\cos(\theta(t)) + F_L(t)\cos(\psi(t) - \frac{\pi}{2}) + F_D(t)\cos(\psi(t)) \\ M\ddot{Z}(t) = -Mg + T(t)\sin(\theta(t)) + F_L(t)\sin(\psi(t) - \frac{\pi}{2}) + F_D(t)\sin(\psi(t)) \\ \ddot{\theta}(t) + 2\xi\omega_n\dot{\theta}(t) + \omega_n^2\theta(t) = \omega_n^2\theta_{in}(t) \end{cases} \tag{1}$$

The system of Ordinary Differentiable Equations (ODEs) above simply describes the motion of the aircraft considered as a rigid body moving on a plane over continuous time t. The mass of the aircraft M takes also into account the mass of its landing gears. Notice that, since the angle $\psi(t)$ (airflow direction angle) can be derived as shown further in this section, the motion of the system can be fully described by means of three coordinates:

- Longitudinal displacement of the aircraft's center of gravity: $X(t)$
- Vertical displacement of the aircraft's center of gravity: $Z(t)$
- Pitch angle: $\theta(t)$

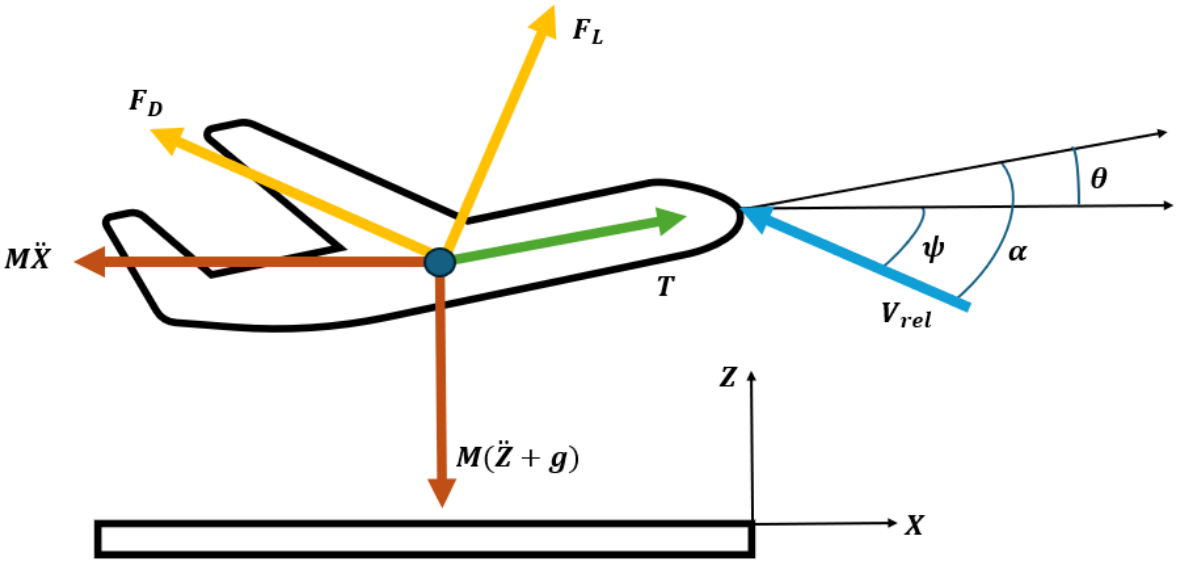

Figure 1: Flight model scheme

The dynamics of the pitch angle are assumed to be ideally controlled, therefore they have been modeled as an asymptotically stable linear system of the second order where ω_n is the natural frequency of the system and ξ is its damping ratio. Other terms in (1) are the thrust force $T(t)$, directed as the pitch angle θ, the cloche command $\theta_{in}(t)$ and the drag and lift forces acting on the airplane, $F_D(t)$ and $F_L(t)$ respectively.

The expressions of the aerodynamic forces are the following:

$$F_L(t) = \frac{1}{2}\rho S c_L(\alpha, u_L) V_{rel}^2$$

$$F_D(t) = \frac{1}{2}\rho S c_D(c_L, u_D) V_{rel}^2$$

where ρ is the air density, S is the frontal surface of the aircraft and V_{rel} is the relative airflow velocity. As the wind velocity has been disregarded, V_{rel} in this instance just represents the aircraft's velocity in absolute value. To make the model simpler, the impact of the pitch angle on the relative velocity has also been neglected. The analysis of aerodynamic forces is incomplete without considering the geometry of the problem. Certain angles must be defined to accurately describe the interaction between the aircraft and the airflow:

- Airflow direction $\psi(t)$, i.e. the direction of the relative speed between the aircraft and the air. It also indicates the directions of the drag and lift forces as described in (1).
- Angle of attack $\alpha(t)$, i.e. the angle between the chord line of the wing and the direction of the airflow.

The functions below geometrically define these angles and the norm of the relative velocity based on the independent coordinates and their derivatives:

$$\psi(t) = atan2(-\dot{Z}(t), -\dot{X}(t))$$

$$\alpha(t) = \theta(t) - atan\left(\frac{-\dot{Z}(t)}{-\dot{X}(t)}\right)$$

$$V_{rel} = \sqrt{\dot{X}(t)^2 + \dot{Z}(t)^2}$$

Then, the drag and lift coefficients, c_D and c_L respectively, have been made dependent on the aircraft's attack angle α. Notice that these coefficients have been also made dependent on two control inputs: u_D, $u_L \in [0, 1]$. As stated before, this allows to model the interaction between the aerodynamic forces and the control surfaces in a simplified manner. How coefficients c_L and c_D vary is further detailed in 2.2.1 while values for all other parameters can be found in Table 2 of the Appendix.
For easiness of future representation, the state and input vectors are defined as:

$$\mathbf{z}_f(t) = \begin{bmatrix} X(t) \\ \dot{X}(t) \\ Z(t) \\ \dot{Z}(t) \\ \theta(t) \\ \dot{\theta}(t) \end{bmatrix} \quad \mathbf{u}_f(t) = \begin{bmatrix} T(t) \\ F_L(t) \\ F_D(t) \\ \theta_{in}(t) \end{bmatrix}$$

so that the system of equations described in (1) can be re-written in a more compact state-space form as:

$$\dot{\mathbf{z}}_f(t) = \mathbf{f}_f\left(\mathbf{z}_f(t), \mathbf{u}_f(t)\right) \tag{2}$$

2.2.1 Aerodynamic Coefficients

As previously discussed, the equations of aerodynamic forces depend on the attack angle and the influence of the aircraft's control surfaces has been modeled as an effect which directly modifies the aerodynamic coefficients using u_L and u_D. Therefore, the need to model suitable relations between these control variables and how they affect the values for the drag and lift coefficients is of the utmost importance. The model for the lift coefficient has been chosen as linear with respect to the angle of attack α. This choice was made because the actual relation between the angle of attack and the lift coefficient is linear for values of $\alpha \in [-20°, 20°]$. The relation becomes nonlinear only when the stall angle is reached. This is not a normal operating condition for an aircraft and therefore it has not been captured in the proposed model.
The action of u_L has the effect of modifying the slope of the linear characteristic causing the wing to generate larger forces for the same value of the angle of attack.
On the other hand, the drag coefficient model depends on the lift coefficient and on the control variable u_D. The drag polar provides the relationship between lift and drag, splitting the overall drag coefficient into two parts: an offset c_{D0} and a function depending quadratically on the lift coefficient through a constant $\phi > 0$ modeling the cross-influence that exists between drag and lift forces. Since control can already act on the drag through the lift, the action of u_D is limited to modifying c_{D0}, allowing the control system to, at most, double the original value for this quantity.
For the sake of completeness, the equations below show the actual implementation:

$$c_L(\alpha, u_L) = c_{L0} + \Delta c_{L,max}[1 - c_{L,var}(1 - u_L)]\alpha \tag{3}$$

$$c_D(c_L, u_D) = c_{D0}(1 + u_D) + \phi\, c_L^2(\alpha, u_L) \tag{4}$$

From equation (3) it is clear that the effect of u_L is to modify the slope of the linear characteristic which defines the relation between the lift coefficient and the attack angle; $\Delta c_{L,max}$ represents the maximum achievable slope for the linear relation while $c_{L,var} \in [0, 1]$ is the normalized maximum slope decrement and c_{L0} is the value for the lift coefficient in case of zero angle of attack. Figure 2 further clarifies this model.
The first part of equation (4) shows that by increasing u_D one can increase the value for the drag coefficient c_D therefore increasing the drag force on the aircraft. This models the effect that air-brakes have on a real airplane.

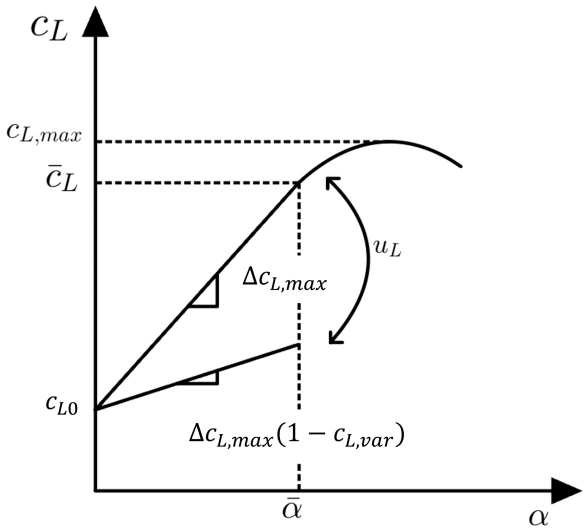

Figure 2: Lift coefficient in relation with the angle of attack. Notice how the effect of the control input u_L is to modify the slope of the linear part of the characteristic as it varies from zero to one

2.3 Ground Model

Once the aircraft touches the ground, its longitudinal, vertical and pitching dynamics still need to be captured. To this extent, the airplane behavior on the runway has been designed using modified versions of the models described in [2] and [3]. While these two publications consider all the six degrees of freedom of the aircraft on the runway, in this treatise only longitudinal, vertical and pitching motion have been considered. Landing gears have been modeled as a parallel of a spring, damper and an actuator thus realizing an active suspension system. The resulting model resembles that of a half-car and the equations of motion have been reported in the following:

$$\begin{cases} M\ddot{X}(t) = -F_B(t) + T(t)\cos(\theta(t)) + F_L(t)\cos(\psi(t) - \frac{\pi}{2}) + F_D(t)\cos(\psi(t)) \\ M\ddot{Z}(t) = -Mg - F_{S_r}(t) - F_{S_{fr}}(t) + T(t)\sin(\theta(t)) + F_L(t)\sin(\psi(t) - \frac{\pi}{2}) + F_D\sin(\psi(t)) \\ J_z\ddot{\theta}(t) = -aF_{S_{fr}}(t) + bF_{S_r}(t) \end{cases} \tag{5}$$

As stated before, mass M takes into account the inertial effect of both the aircraft's fuselage and landing gears while the elastic and damping properties of the airplane wheels have been neglected for simplicity.
$F_{S_{fr}}(t)$ and $F_{S_r}(t)$ represent the front and rear suspension total force, respectively.
These forces can be written as:

$$F_{S_r}(t) = 2k_r(Z(t) - b\ sin(\theta(t)) - \Delta_r) + 2F_{Ar}(t) + 2c(\dot{Z}(t) - b\ cos(\theta(t))\dot{\theta}(t)) \tag{6a}$$

$$F_{S_{fr}}(t) = k_{fr}(Z(t) + a\ sin(\theta(t)) - \Delta_{fr}) + F_{Afr}(t) + c(\dot{Z}(t) + a\ cos(\theta(t))\dot{\theta}(t)) \tag{6b}$$

where k_{fr} and k_r represent the front and rear suspension stiffness, c is the damping and Δ_{fr} and Δ_r are the front and rear pre-load.
Notice that, also in this case, the motion of the system is described by three independent coordinates yielding a state space realization of dimension six.
With respect to the model described in 2.2, three more control inputs were added: $F_B(t)$ models the braking force applied on the wheels of the aircraft while $F_{Afr}(t)$ and $F_{Ar}(t)$ represent the front and rear active suspension forces respectively. Other parameters in (5) and (6) include the aircraft's pitching moment of inertia J_z and the distances of the rear and front landing gears from the airplane's center of mass, denoted with b and a respectively.

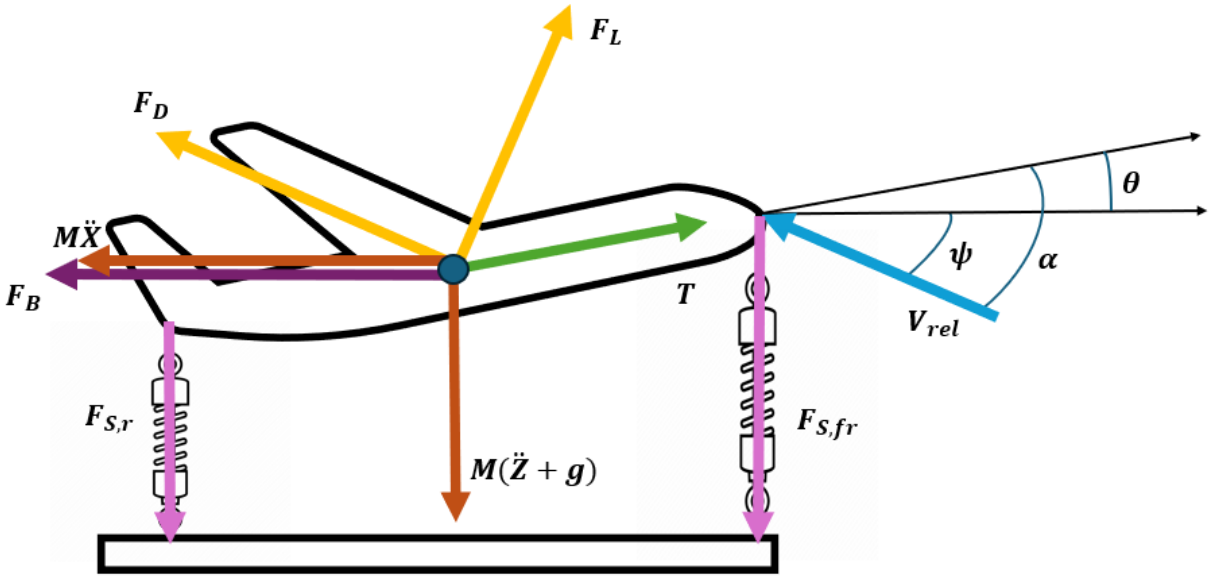

Figure 3: Ground model scheme

Again, by defining the state and input vector for this system as:

$$\mathbf{z}_g(t) = \begin{bmatrix} X(t) \\ \dot{X}(t) \\ Z(t) \\ \dot{Z}(t) \\ \theta(t) \\ \dot{\theta}(t) \end{bmatrix} \qquad \mathbf{u}_g(t) = \begin{bmatrix} F_B(t) \\ T(t) \\ F_L(t) \\ F_D(t) \\ F_{Afr}(t) \\ F_{Ar}(t) \end{bmatrix}$$

the system of ODEs described in 5 can be simplified and re-written in state space form as:

$$\dot{\mathbf{z}}_g(t) = \mathbf{f}_g\left(\mathbf{z}_g(t), \mathbf{u}_g(t)\right) \tag{7}$$

2.4 Combined Switching Model

Switching between the aircraft's in-flight dynamics and its ground dynamics becomes necessary to completely depict the landing procedure. Therefore, a simple switching model has been derived employing equations (2) and (7) and is schematically described by the hybrid automaton represented in Figure 4.

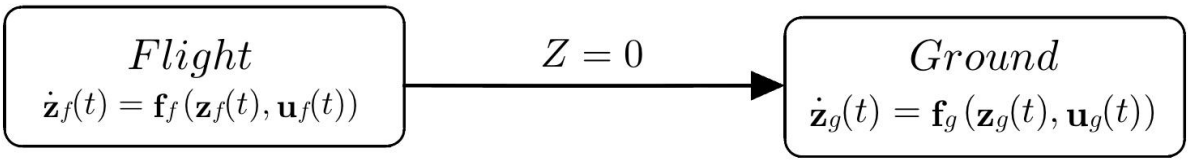

Figure 4: Hybrid automaton of the complete system

The simulator switches from the flight to the ground model once the center of gravity of the aircraft reaches the value of zero. Once this happens, this system is blocked from going into flight mode again

and continues to evolve indefinitely following the dynamics described by the model of the airplane on the ground. Notice that, since the state vectors of both models coincide, the final state registered while the aircraft is completing the descent phase is passed as the initial state to the ground model. This allows to simulate quite well the impact of the airplane on the ground upon landing.

2.5 Simulation

To simulate the model, numerical integration techniques are employed. First, a variable step integration method (ode45) is used; the obtained results are then compared with the ones obtained using the fixed step method Runge-Kutta-2 (RK2). Since the results obtained match quite well, the latter method can be employed to simulate the model at the advantage of a lower computational cost.

2.5.1 Results

All the following results are obtained by integrating the model equations with RK2 using a sampling time $T_s = 0.01$ s. A predefined sequence of control input is used to simulate the landing procedure of the airplane.

The first thing to be assessed is the aircraft's behavior during the descent phase and upon touchdown:

(a) Aircraft descent trajectory

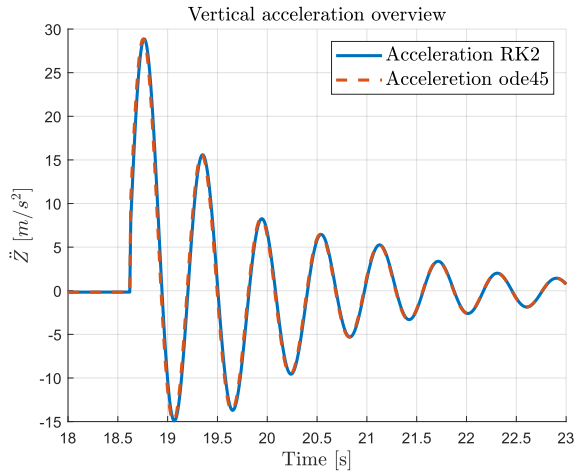

(b) Vertical acceleration at touchdown

Figure 5

As it can be seen from Figure 5a, the descent trajectory well approximates that of a real aircraft while Figure 5b shows that, at the moment of the impact with the ground, vertical accelerations have a non-negligible magnitude.

In the following, a numerical optimization-based approach to control the landing phase is proposed. The goal is to complete the procedure while also trying to contain as much as possible the accelerations arising due to the impact on the ground.

3 Finite Horizon Optimal Control

As stated before, the goal of this project is to optimize the comfort for the passengers. Having selected RK2 as numerical integration technique, the system equations can now be discretized. Thus, the evolution of the state vectors in discrete time can be described through the following compact notations:

$$\mathbf{z}_f(k+1) = \bar{\mathbf{f}}_f\left(\mathbf{z}_f(k), \mathbf{u}_f(k)\right) \tag{8a}$$

$$\mathbf{z}_g(k+1) = \bar{\mathbf{f}}_g\left(\mathbf{z}_g(k), \mathbf{u}_g(k)\right) \tag{8b}$$

where $k \in \mathbb{N}$ is the discrete time variable.
Having done these considerations an optimization problem is formulated.

3.1 Optimization Problem

The optimization problem consists of a Finite Horizon Optimal Control Problem (FHOCP), which tries to minimize the acceleration generated during the entire landing procedure.
This is so because the comfort of the passengers is strictly related to the accelerations to which the body is subjected. Of course, a correct and safe landing procedure must be guaranteed.
In doing so, the following optimization problems are stated:

Flight Optimization:

$$\min_{\mathbf{U}_f} \quad \sum_{k\in H} (W_Z \ddot{Z}(k)^2 + W_\theta \ddot{\theta}(k)^2 + W_X \ddot{X}(k)^2) \tag{9a}$$

s.t.

$$\mathbf{z}_f(k+1) = \bar{\mathbf{f}}_f(\mathbf{z}_f(k), \mathbf{u}_f(k)) \quad \forall k \in H, \tag{9b}$$

$$\mathbf{z}_f(0) = \mathbf{z}_{f0}, \tag{9c}$$

$$-\mathbf{RL}_f \leq \mathbf{u}_f(k+1) - \mathbf{u}_f(k) \leq \mathbf{RL}_f \quad \forall k \in H, \tag{9d}$$

$$\mathbf{U}_{lb} \leq \mathbf{U}_f \leq \mathbf{U}_{ub}, \tag{9e}$$

$$Z(k) \geq 0 \quad \forall k \in H, \tag{9f}$$

$$X_{lb} \leq X_{end} \leq X_{ub}, \tag{9g}$$

$$\tilde{\mathbf{z}}_{f,end} = \tilde{\mathbf{z}}_{ref} \tag{9h}$$

Ground Optimization:

$$\min_{\mathbf{U}_g, \mathbf{z}_{g0}} \quad \sum_{k\in J} (W_Z \ddot{Z}(k)^2 + W_\theta \ddot{\theta}(k)^2 + W_X \ddot{X}(k)^2) \tag{10a}$$

s.t.

$$\mathbf{z}_g(k+1) = \bar{\mathbf{f}}_g(\mathbf{z}_g(k), \mathbf{u}_g(k)) \quad \forall k \in J, \tag{10b}$$

$$\mathbf{z}_g(0) = \mathbf{z}_{g0}, \tag{10c}$$

$$\mathbf{z}_{lb} \leq \mathbf{z}_{g0} \leq \mathbf{z}_{ub}, \tag{10d}$$

$$-\mathbf{RL}_g \leq \mathbf{u}_g(k+1) - \mathbf{u}_g(k) \leq \mathbf{RL}_g \quad \forall k \in J, \tag{10e}$$

$$\mathbf{U}_{lb} \leq \mathbf{U}_g \leq \mathbf{U}_{ub}, \tag{10f}$$

$$X_{lb} \leq X_{end} \leq X_{ub}, \tag{10g}$$

$$\dot{\mathbf{z}}_{g,end} = 0, \tag{10h}$$

$$Z_{end} = 0, \tag{10i}$$

$$\theta_{end} = 0 \tag{10j}$$

where H and J are the sets of discrete time instants for the flight and ground model simulations respectively. The variables $\mathbf{U}_f$ and $\mathbf{U}_g$ collect the vector of inputs in flight and ground mode at each

time step during the entire simulation. Moreover in the ground optimization procedure also the initial time instant is taken as an optimization variable and computed respecting suitable physical bounds given by constraint (10d). Details of this choice are explained in 3.2.

The weights W_Z, W_X and W_θ, emphasize the relevant states for the optimization purpose and normalize the state variables to a common range based on their potential values. Notice that the same values were used for both optimization problems.
Most of the constraints used in the optimization procedures are identical, except for the ones expressed in (10d) and the differences in the terminal conditions (9h) and (10h)-(10i)-(10j). Thus, it is enough to explain the constraints for the first problem to understand the respective constraints for the second. Just a simple change in the notation is implemented.

First, the dynamic equation is enforced at each time step by (9b) and the initial value is taken into account by (9c). While the initial ground condition is an optimization variable, for the flight the aircraft is considered during the descending phase. Thus the following vector has been selected:

$$\mathbf{z}_{f0} = \begin{bmatrix} 0 & 100 & 50 & -5 & 0 & 0 \end{bmatrix}^T$$

where 50 is the initial height in meters, while 100 and -5 are respectively the initial longitudinal and vertical velocities in meters per second.

Constraints (9d)-(9e) respectively control the rate at which the input influences the system and impose limits on the actuator by setting upper and lower bounds on the input.
The rate limiter is implemented as a linear constraint and involves all the actuators used during the entire landing procedure. Then the two constraints (9f)-(9g) limit the aircraft to respect some bounds on the vertical position, preventing the height from being negative during the entire flight procedure, and on the longitudinal position to reach a final location within a certain region. Indeed, the runway has been considered to be 2 kilometers long, starting at a distance of 1000 meters relative to the initial horizontal position of the airplane. Hence, for the flight optimization, this constraint forces the aircraft to touchdown within a certain region of the runway, while for the ground optimization, to stop before the end of the landing strip.

Lastly, termination conditions are implemented in (9h) and (10h). For the ground problem, it represents the required equilibrium condition at the end of the landing, thus the vector of the final derivative of the state $\dot{\mathbf{z}}_{g,end}$ is set to zero. Moreover, conditions on the final height and pitch are enforced in (10i) and (10j). On the other hand, for the flight phase, it enforces the matching condition between the two optimization routines imposing a reference $\tilde{\mathbf{z}}_{ref}$ for the final flight state $\tilde{\mathbf{z}}_{f,end}$. Notation with the tilde denotes the state without the X coordinate, this is required since the matching condition is implemented as a constraint for all the states except the longitudinal position. The reason for this is that once both (9g) and (10g) are respected, the longitudinal coordinate of the touchdown does not matter. Further details on the choice of $\tilde{\mathbf{z}}_{ref}$ can be found in section 3.2.

3.2 Main issues of the optimization problem

A few observations help to understand how the emerging problems are handled concerning the optimization process.

- *Sub-Optimality*: Managing the transition between the flight and ground models is one of the most difficult aspects of the simulating landing process and this difficulty also shows up in the optimization problem. Indeed, the flight-ground switching design necessitates a meticulous choice of the optimization method to minimize sources of sub-optimality while ensuring a fair computational time. These reasons suggest that the general optimization issue should be divided into two sub-problems, each pertaining to a single model at a time. This approach allows the solver to run two different subroutines reaching the optimal trajectory for each of the two models.

However, the two distinct optimal trajectories for the flight and ground phase lead to an overall unfeasible and sub-optimal trajectory. To cope with this issue, some concepts of Bellman's principle have been exploited. The idea is to run the ground subroutine before the flight. In doing so, also the initial condition of the ground trajectory is chosen by the solver to guarantee the best possible trajectory for the touchdown and ground deceleration phases, as these are the most critical for ensuring passenger comfort. Hence, the optimal initial condition found for the ground also defines the target state for the flight optimization forcing a coherent optimal transition between the two different regimes of operation. Once such a target is computed, the flight subroutine is carried out and the whole trajectory can be reconstructed by the union of the two previous optimal results. To sum up, this means that $\tilde{\mathbf{z}}_{ref}$ for the flight coincides with the optimal $\tilde{\mathbf{z}}^*_{g0}$ computed in the ground optimization, which, as already discussed, is the full optimal initial state, except for the longitudinal coordinate.

- *Trajectory conjunction*: In addition to the sub-optimality issue, it is important to remark that the match between the two trajectories is not an easy task due to the physical limitations of the problems themselves and those coming from the modeling choices. The latter ones, for instance, force the ground optimization to prefer zero pitch initial condition, which instead, is unfeasible for the flight dynamics, unless very high landing speeds are allowed. This is confirmed by real experience since an aircraft needs to operate a flare maneuver in order to slow down the vertical speed and reach a softer and safer touchdown. For this reason, some constraints regarding the initial ground condition are added and, through a proper gridding and trial-and-error of these limitations, these constraints are tuned to achieve the best performance.

- *High computational load*: It is immediately evident that there are numerous inputs involved. This causes the complexity of the optimization problem to scale up rapidly with the considered sampling time and control horizon. A reasonable approach to tackle this issue is not to update the input sequence at each new time instant of the simulation but to set a suitable down-sampling logic. This implies that once a certain value is selected for an input, then it must be kept constant for a predetermined amount of time. In this way, the number of control variables is reduced, as is the computational effort. Remarkable is the fact that different control actions about various actuators can be re-computed at different frequencies. For instance, the frequency at which the active suspension actuators must be adjusted differs from that of the thrust in the ground optimization.

3.3 Final Solution

This section focuses on the solution to the two previously proposed optimization problems. In particular, the procedure that has been followed to tackle the problem is composed of two main phases:

1. Unconstrained Optimization: both problems are solved not accounting for the presence of constraints

2. Constrained Optimization: constraints on states and control variables are considered

In both cases, iterative solution algorithms are employed. A more detailed description of the solver settings is found in the following sections.

3.3.1 Unconstrained Optimization

In this case, the employed iterative algorithm will try to satisfy the following sufficient optimality condition:

$$\nabla_{\mathbf{U}} f(\mathbf{U}) = 0 \tag{11}$$

Where $f(\mathbf{U})$ denotes generically the cost function of both the problems at hand.
In order to be able to numerically evaluate the condition stated by (11), the gradient of the cost is required. In this case, the value for $\nabla_{\mathbf{U}} f(\mathbf{U})$ is obtained numerically using Central Finite Differences

using a step of 2^{-17}.

The Hessian of the cost would be necessary to calculate the search direction. In both cases, however, the cost function is a sum of squared values. This means that the Gauss-Newton method can be employed to compute the search direction without having to compute the Hessian of the cost.

Finally, a backtracking line-search sub-routine with Armijo conditions is employed to compute the step length at each iteration.
Once the optimal control sequences are computed, they are applied to the models derived in sections 2.2 and 2.3. Optimization routine results are shown in 3.3.4.

3.3.2 Line Search Parameters

Parameter	Symbol	Value
Termination tolerance on the norm of the directional derivative	TOL_{∇}	10^{-6}
Termination tolerance on the relative improvement of the cost function	TOL_{fun}	10^{-12}
Termination tolerance on the relative change of optimization variables	TOL_x	10^{-12}
Maximum number of iterations	N_{max}	50

Table 1: List of termination tolerances

The termination tolerances used in the unconstrained problem are reported above in Table 1.
The TOL_{∇} has been chosen considering the accuracy of the Central Finite Difference method relative to the value of the cost function experienced in different simulations.
The maximum number of iterations instead, has been selected as a good trade-off between a faster simulation and a sufficiently small cost function.
While specific parameters were adjusted, others were left unchanged based on their theoretical validity and established effectiveness, thanks to different experiments.
Note that the same parameters were used in both, ground and flight, optimizations.

3.3.3 Barrier Functions

The main issue with using the unconstrained approach is that constraints are not directly implemented into the optimization process. However, some of them are necessary to achieve results consistent with the realistic behavior of an aircraft landing. For this reason, a selection of constraints has been added through the barrier function method explained in the following lines.
As a matter of fact, for what concerns unconstrained optimization, the formulation of the program focuses solely on the design of the cost function. Nevertheless, a careful choice of this function is essential to consider constraints while simultaneously exploiting standard unconstrained optimization techniques. To achieve this, constraints are rewritten as penalties added to the cost function that models the primary desired goal. These penalties are represented by suitable barrier functions designed to increase the overall cost value when a constraint is violated.

In the program discussed in this section, exponential barrier functions have been selected to implement constraints regarding the bounds of the inputs and, specifically for the flight scenario, to ensure that the height of the aircraft does not become negative. The expressions below show the structure of the barriers depending on the vectors of suitable hyper-parameters $\boldsymbol{\varepsilon}$ and $\boldsymbol{\zeta}$.

$$\boldsymbol{\varepsilon} = \begin{bmatrix} \boldsymbol{\varepsilon}_u \\ \boldsymbol{\varepsilon}_{IC} \\ \varepsilon_Z \end{bmatrix}, \quad \boldsymbol{\zeta} = \begin{bmatrix} \zeta_u \\ \zeta_{IC} \\ \zeta_Z \end{bmatrix}$$

For the ground program, violations of both input and initial condition bounds have been penalized:

$$\sum_{k \in J} \boldsymbol{\varepsilon}_u^T \cdot e^{-2\zeta_u \cdot diag([\mathbf{u}_g(k) - \mathbf{u}_{lb}(k)])} \cdot \boldsymbol{\varepsilon}_u$$

$$\sum_{k\in J} \boldsymbol{\varepsilon}_u^T \cdot e^{-2\zeta_u \cdot diag([\mathbf{u}_{ub}(k)-\mathbf{u}_g(k)])} \cdot \boldsymbol{\varepsilon}_u$$

$$\boldsymbol{\varepsilon}_{IC}^T \cdot e^{-2\zeta_{IC} \cdot diag([\mathbf{z}_{g0}-\mathbf{z}_{lb}])} \cdot \boldsymbol{\varepsilon}_{IC}$$

$$\boldsymbol{\varepsilon}_{IC}^T \cdot e^{-2\zeta_{IC} \cdot diag([\mathbf{z}_{ub}-\mathbf{z}_{g0}])} \cdot \boldsymbol{\varepsilon}_{IC}$$

For the flight phase, the same barriers have been added to the inputs over the period defined by H. In addition, also negative heights for all the flight duration have been penalized as follows:

$$\sum_{k\in H} \varepsilon_z^2 \cdot e^{-2\zeta_z Z(k)}$$

As the expression suggests, elements in $\boldsymbol{\varepsilon}$ must be kept as small as possible to avoid misleading effects on solutions that satisfy the constraints, while those in $\boldsymbol{\zeta}$ must be large to rapidly penalize even small violations. Moreover, since the overall cost function becomes multi-objective, these weights have been chosen carefully to maintain equilibrium with the minimization of the primary cost function.

Finally, the quadratic structure has been maintained to enable the solver to implement a Gauss-Newton method in the approximation of the Hessian.

While barrier function methods have been exploited to represent inequality constraints on the optimization variables, a different approach has been chosen to implement the matching condition between flight and ground optimization routines. As enforcing this match would normally require an equality constraint, it has been decided to add a penalization on the termination condition of the flight optimization. Hence, a matrix weighting the difference between the final state of the flight and the reference built via the ground optimization is added. With the same approach, the termination conditions for the ground have been implemented.
To be precise, the unconstrained cost function for both problems has the following structure:

$$\min_{\mathbf{U}_f} \quad \sum_{k\in H} (W_Z \ddot{Z}(k)^2 + W_\theta \ddot{\theta}(k)^2 + W_X \ddot{X}(k)^2) + (\tilde{\mathbf{z}}_{f,end} - \tilde{\mathbf{z}}_{ref})^T W_{f,end} (\tilde{\mathbf{z}}_{f,end} - \tilde{\mathbf{z}}_{ref}) + \Lambda_f \tag{12}$$

$$\min_{\mathbf{U}_g,\, \mathbf{z}_{g0}} \quad \sum_{k\in J} (W_Z \ddot{Z}(k)^2 + W_\theta \ddot{\theta}(k)^2 + W_X \ddot{X}(k)^2) + \dot{\mathbf{z}}_{g,end}^T W_{g,end} \dot{\mathbf{z}}_{g,end} + W_{g,end}(Z_{end}^2 + \theta_{end}^2) + \Lambda_g \tag{13}$$

where Λ_g and Λ_f collect the overall barrier function contribution.

Difficulties in fine-tuning and balancing the resulting multi-objective unconstrained cost function with barrier methods have prevented the achievement of satisfactory results and represent one of the main reasons to prefer a constrained approach.

3.3.4 Unconstrained Optimization Results

The first thing it is notable to evaluate is whether the proposed model for the aircraft simulates well the landing procedure with the given inputs from the optimization procedure. Combining the information about the longitudinal and vertical position it is possible to obtain the aircraft descent trajectory, as shown in Figure 6. Figure 7 instead, shows the accelerations to which the plane is subjected.

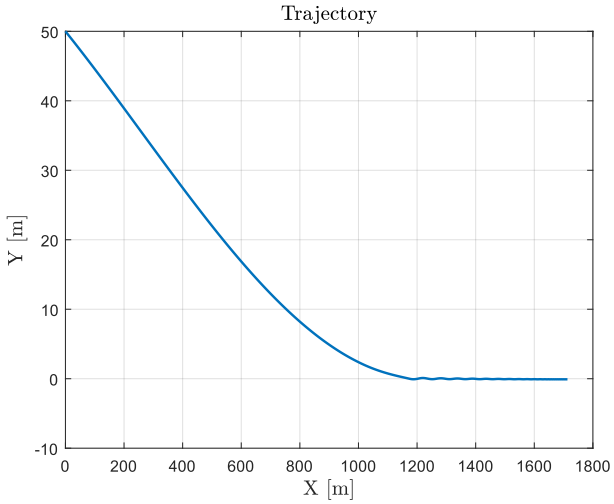

Figure 6: Aircraft trajectory resulting from the unconstrained optimization routine

A high peak in the accelerations, around twelve seconds is registered due to the impact with the ground. These accelerations exceed consistently the average values of a modern landing procedure. This suggests proceeding with a constrained approach.

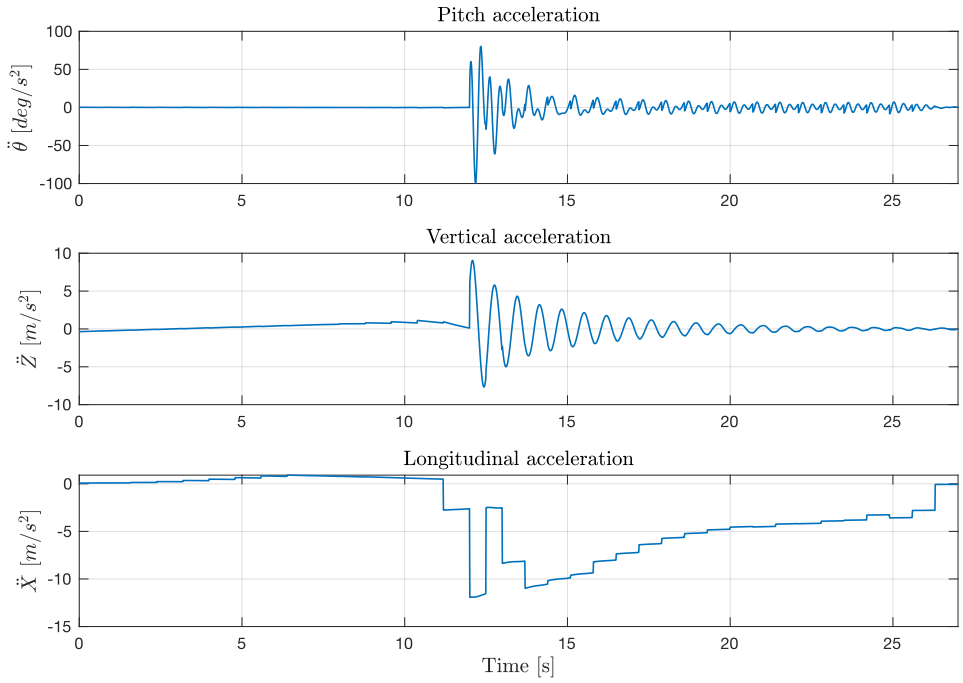

Figure 7: Vertical, Pitch and Longitudinal accelerations resulting from applying the solution from the unconstrained problem

3.3.5 Constrained Optimization

The method employed to deal with the constrained problem is the Sequential Quadratic Programming (SQP). This is an iterative approach that approximates the non-linear program (NLP) into a quadratic program (QP) at each iteration j. The SQP aims to create a sequence (x^j, λ^j, μ^j) which converges to a Karush-Kuhn-Tucker (x^*, λ^*, μ^*) triplet corresponding to a local minimizer.

As such, an iterative process of formulating a QP from the NLP is required. Thanks to the fact that the cost functions are in quadratic forms, the Constrained Gauss-Newton approach provides an efficient way to construct the QP hessian at each iteration. To deal with the QP resolution the interior point approach is used. Due to the high number of optimization variables in this particular scenario, this approach has a significant computational advantage over the active set. Solving the QP results in the search direction p^{j^*} and the Lagrange multipliers $\tilde{\lambda}^{j^*}$, $\tilde{\mu}^{j^*}$. These are used to compute the triplet at the $j+1$ iteration:

Finally the computation of the step length t^j is required. To do so, the ℓ_1-norm merit function has to be defined. Thanks to the structure of this function is possible to avoid the violation of the constraints by performing an unconstrained back-tracking line-search with Armijo stopping condition. This approach guarantees a global convergence of the SQP algorithm. For further details refer to [4].

Regarding the parameters, the optimization solver values remain identical to those used in the unconstrained case with the same considerations. In addition to these, a default constraint tolerance of $TOL_{constr} = 10^{-6}$ has to be added to the parameters listed in Table 1.

3.3.6 Constrained Problem Refinements

The overall structure of the optimization problem remains the same as in the one discussed in section 3.1, but some adjustments are implemented to improve the solution.
The first adjustment is to consider constraints on the height of the aircraft during the flight phase only within a limited period $H_Z \subset H$ around the contact with the ground. This choice reduces the number of nonlinear constraints the solver needs to evaluate, thereby speeding up computations. Additionally, given the problem's structure, which aims to limit the accelerations and dynamics of the aircraft, this limited set of constraints is sufficient to prevent negative heights during flight. Therefore, constraint (9f) in section 3.1 is replaced by the following:

$$Z(k) \geq 0 \quad \forall k \in H_Z \tag{14}$$

The second refinement concerns the ground cost function. It includes an additional weight W_{add} penalizing the height during the ground phase to help the aircraft recover a horizontal position faster, thus limiting the time the nose is pitched down. This weight is active just over a subset of the overall ground phase period $J_{add} \subset J$, representing the second half of J. The final cost function results in:

$$\min_{\mathbf{U}_g,\, \mathbf{z}_{g0}} \quad \sum_{k \in J} (W_Z \ddot{Z}(k)^2 + W_\theta \ddot{\theta}(k)^2 + W_X \ddot{X}(k)^2) + \sum_{k \in J_{add}} W_{add} Z(k)^2 \tag{15}$$

3.3.7 Results and Observations

The solution found by the solver represents a dynamic closely resembling a real landing approach. The trajectory (Figure 8a) shows a gradually descending phase while approaching the runway and then stopping far before the ending.

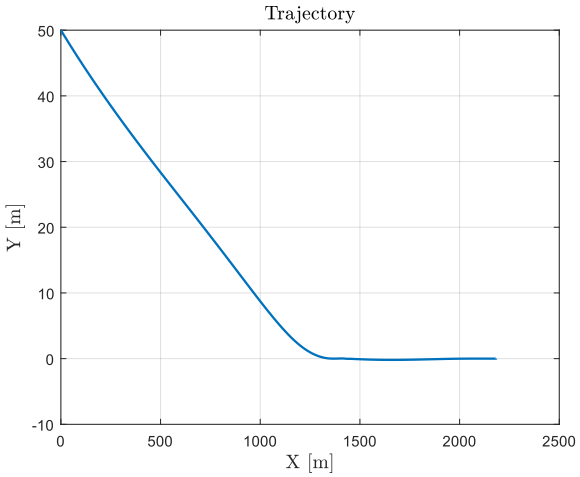

(a) Constrained Aircraft trajectory

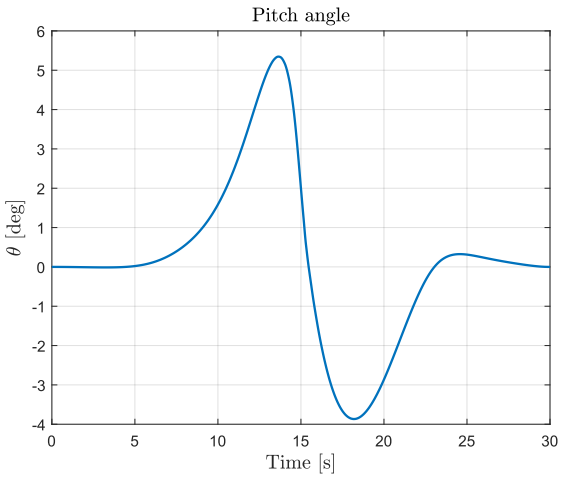

(b) Flare Maneuver

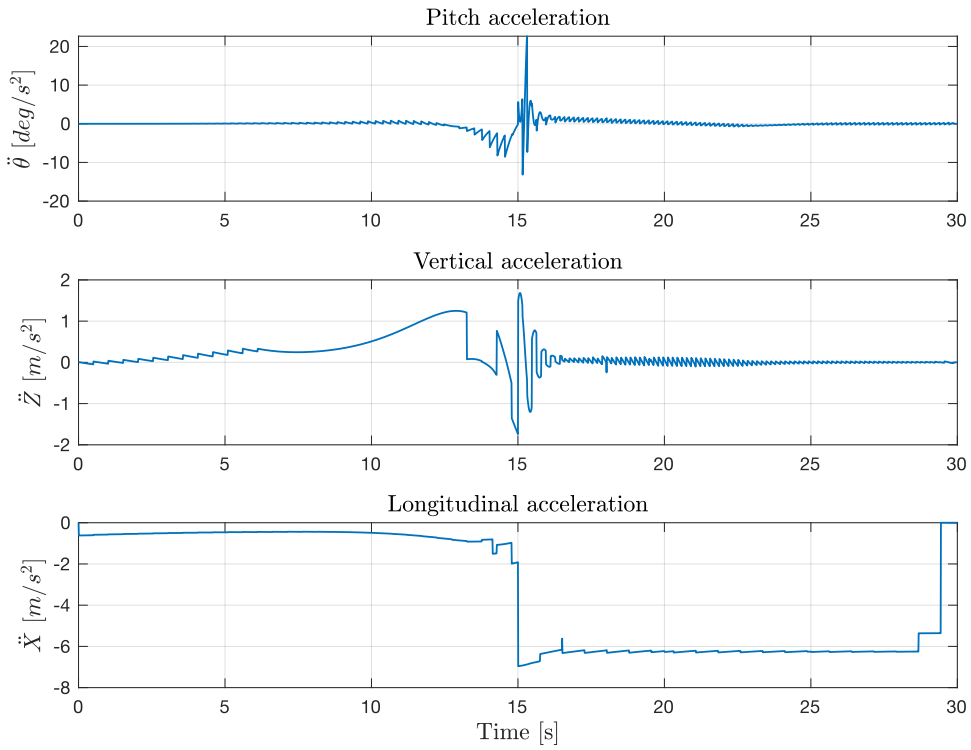

(c) Vertical, Pitch and Longitudinal accelerations resulting from applying the solution from the constrained problem

Figure 8: Constrained Optimization Results

The accelerations experienced during the landing procedure are maintained within typical flight levels. As illustrated in Figure 8c, ground impact at 15 seconds significantly increased overall acceleration, making the aircraft reach the peak at this instant. Compared to the unconstrained case, the peaks of the pitch, vertical and longitudinal accelerations have been reduced respectively by 75%, 80% and 40%. In addition, substantial progress is achieved in attenuating also post-impact accelerations resulting in an overall solid improvement for the passenger's comfort.

Regarding the inputs, the aerodynamic forces are accurately modeled by their associated coefficients and controlled by optimal commands (Figure 9), these influence the aircraft's dynamics by describing a realistic behavior. As a matter of fact, Figure 8b shows a flare maneuver that is typical of landing and consists of an increase in pitch angle shortly before touchdown. Flaring is pivotal for augmenting the aircraft's surface, thereby enhancing braking and decelerating the aircraft.
Prior to touchdown (at 15 seconds), the solver prioritizes lift over drag, as depicted in Figure 9. To achieve this, the solver dynamically adjusts the pitch angle maximizing the lift. Furthermore, as the aircraft decelerates, both lift and drag forces gradually decrease to zero due to the diminishing relative airspeed.

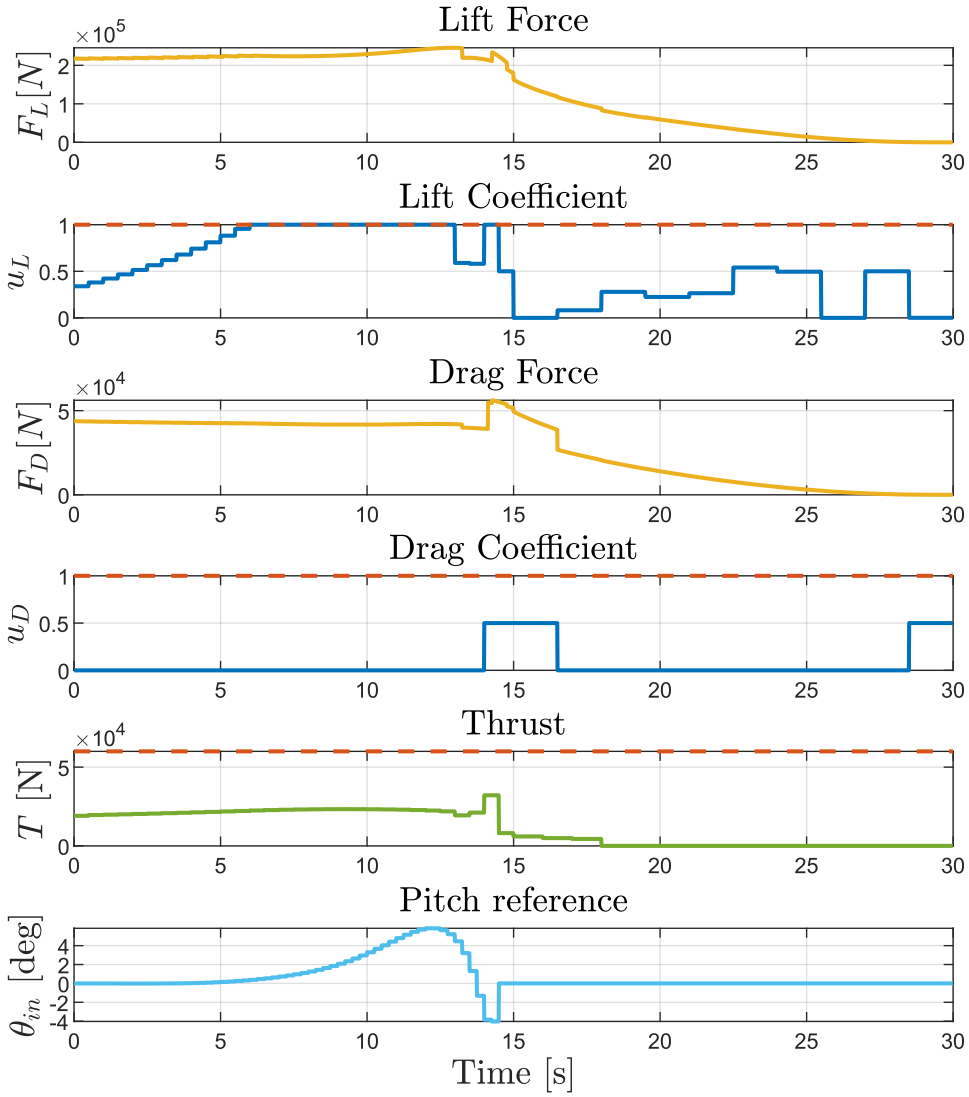

Figure 9: Common inputs to flight and ground phase: thrust (green), lift and drag forces (yellow). Lift and drag forces are represented with the corresponding input coefficients (blue). The pitch reference command (light blue) instead acts only during the flight phase, which ends at 15 seconds. Red dashed lines represent the input upper bounds.

Beyond the effects of aerodynamic forces, other inputs are involved in the simulation and depicted in Figures 9 and 10. The thrust force remains nearly constant during the flight phase to maintain the relative velocity needed to keep the aircraft airborne, but it is quickly turned off after touchdown.

Also, the additional inputs involved only in the touching phase show reasonable behavior. The brake force is kept constant to achieve a nearly constant longitudinal deceleration, while the active suspensions correctly represent the differences due to the variation between the front and rear stiffness values and touchdown with a positive pitch. Indeed, this leads to a higher load on the rear wheels at the touchdown, bringing about higher values for the rear active suspension forces.

Finally, some further comments complete the discussion. First, comparing the trajectories of the aerodynamic coefficients after the touchdown and those of the active suspensions, different down-sampling strategies can be appreciated, improving computational speed.
Then, the other important thing to notice is that the accelerations exhibit a discontinuous behavior. This is due to the discontinuous nature that the inputs have, combined with the down-sampling which has been put in place to reduce the number of unknowns in the two problems.
Since the relation between the inputs and the accelerations is algebraic, if the former presents significant discontinuities the latter will show them too. One possible way to reduce this effect, while keeping the number of optimization variables low, would be to use collocation choosing as unknowns the values for the inputs at a reduced number of time instants and fitting a spline using these via-points. In this way, the inputs are continuous and smooth curves and, consequently also the accelerations will maintain continuity in all points except for the time instant where the aircraft hits the ground and the switch between the two models happens.

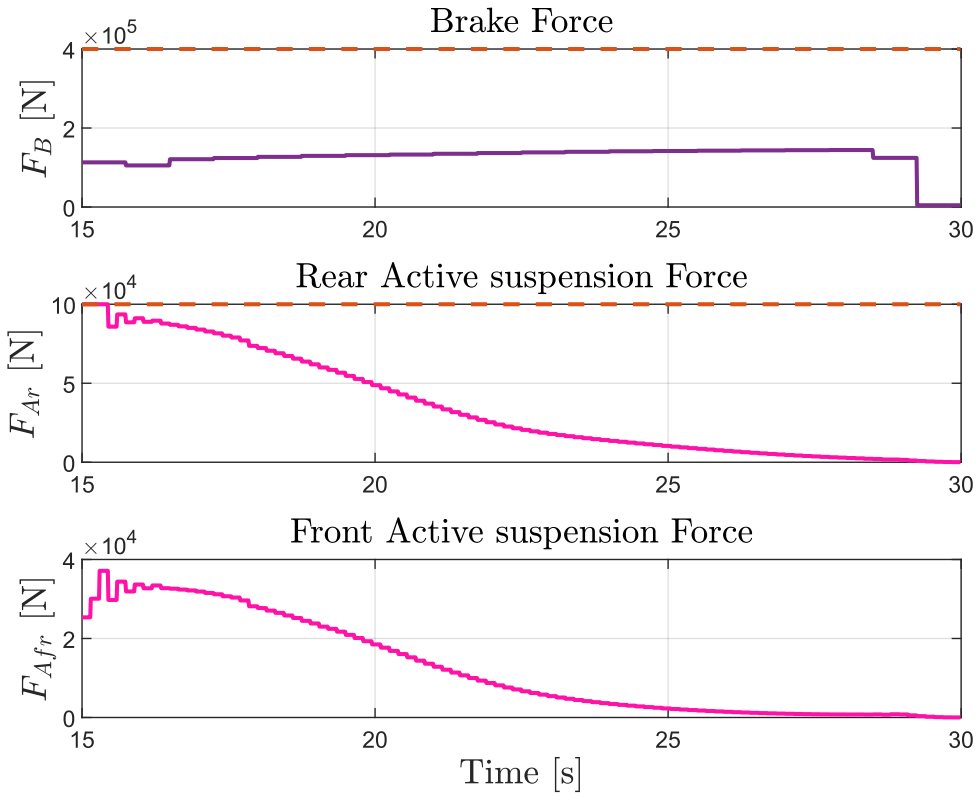

Figure 10: Additional ground inputs, brake (purple), rear and front active suspension forces (pink). In the front case, the bound is not an issue and it is not shown since it is the same as the rear. Since their influence starts with the touchdown, the time scale starts at $15s$.

4 Conclusion

This report demonstrates how to optimize a flight trajectory and the corresponding actuator usage with a constrained optimization approach, aiming to minimize acceleration during the landing phase. Initially a model of the aircraft and of the forces involved has been made.
Then the first tentative approach was made designing an unconstrained problem with barrier functions to implement some of the necessary constraints. This solution, as it is shown, reaches good results but is still unsatisfactory in terms of the passengers' comfort due to the high accelerations deriving from contact with the ground.
This led to the formulation of a constrained problem which finally achieved fully satisfactory results. These outcomes from the Finite Horizon Optimal Control Problem can form the basis for more advanced control strategies, like Model Predictive Control. However, this assumes that challenges such as significant computational demands and dynamic switching between the models can be overcome.

5 Appendix

Symbol	Name	Value	Unit of Measure
M	Aircraft total mass (fuselage and wheels)	$22.39 \cdot 10^3$	kg
J_z	Aircraft pitching moment of inertia	10^5	$kg \cdot m^2$
k_r	Rear spring suspension stiffness	$6.73 \cdot 10^5$	N/m
k_{fr}	Front spring suspension stiffness	$1.59 \cdot 10^4$	N/m
c	Suspension damping	$4.06 \cdot 10^3$	$N \cdot s/m$
L	Aircraft length	10	m
a	Distance from center of gravity to front aircraft end	7.76	m
b	Distance from center of gravity to rear aircraft end	1.94	m
Δ_{fr}	Preload of front landing gear suspension	2.76	m
Δ_r	Preload of the rear landing gear suspension	0.13	m
T_{max}	Maximum thrust force	$6 \cdot 10^4$	N
B_{max}	Maximum braking force	$4 \cdot 10^5$	N
F_{max}	Maximum active suspension force	10^5	N
θ_{max}	Maximum reference of pitch angle	0.17	rad
ω_n	Natural frequency of pitch dynamics for flight mode	1.5	rad/s
ξ	Damping ratio of pitch dynamics for flight mode	0.9	1
c_{L0}	Zero Attack Angle Lift coefficient	0.63	1
$\Delta c_{L,max}$	Maximum achievable slope of the α - c_L characteristic	3.15	1
$c_{L,var}$	Normalized maximum slope decrement	0.2	1
c_{D0}	Drag Coefficient Bias	0.12	1
ϕ	Lift-induced drag coefficient	0.0435	1
S	Aircraft surface	$5 \cdot 10^1$	m^2
g	Gravitational acceleration	9.81	m/s^2
ρ	Air density	1.2	kg/m^3

Table 2: Model Parameters

Symbol	Name	Unit of measure
$X(t)$	Longitudinal position	m
$\dot{X}(t)$	Longitudinal speed	m/s
$\ddot{X}(t)$	Longitudinal acceleration	m/s^2
$Z(t)$	Vertical position	m
$\dot{Z}(t)$	Vertical speed	m/s
$\ddot{Z}(t)$	Vertical acceleration	m/s^2
$\theta(t)$	Pitch angle	rad
$\dot{\theta}(t)$	Pitch angle velocity	rad/s
$\ddot{\theta}(t)$	Pitch angle acceleration	rad/s^2
$\theta_{in}(t)$	Pitch angle command	rad
$\alpha(t)$	Attack Angle	rad
$\psi(t)$	Airflow direction	rad
$T(t)$	Thrust force	N
$F_L(t)$	Lift force	N
$F_D(t)$	Drag force	N
$F_{Ar}(t)$	Rear active suspension force	N
$F_{Afr}(t)$	Front active suspension force	N
$u_L(t)$	Input lift coefficient	
$u_D(t)$	Input drag coefficient	

Table 3: List of Symbols

References

[1] R.C. Nelson. *Flight Stability and Automatic Control*. Aerospace Science & Technology. WCB/McGraw Hill, 1998.

[2] Hakan Yazici and Mert Sever. Observer based optimal vibration control of a full aircraft system having active landing gears and biodynamic pilot model. *Shock and Vibration*, 2016:1–20, 01 2016.

[3] Shifu Liu, Jianming Ling, Yu Tian, and Tianxin Hou. Evaluation of aircraft random vibration under roughness excitation during taxiing. *International Journal of Transportation Science and Technology*, 2023.

[4] Lorenzo Fagiano. Constrained numerical optimization for estimation and control. Lecture Notes, 2023. M.Sc. Programme in Automation and Control Engineering, Course 052358, Version 1.1, December 22, 2023.